Decoupling impacts of weather conditions on interannual variations in concentrations of criteria air pollutants in south China – constraining analysis uncertainties by using multiple analysis tools

Yu Lin[1], LeimingZhang[2*], Qinchu Fan[3], He Meng[4], Yang Gao[1,3,5], Huiwang Gao[3,5], Xiaohong Yao[1,3,5*]

5 [1]Sanya Oceanographic Institution (Ocean University of China), Yazhou Bay Science & Technology City, Sanya, China
[2]Air Quality Research Division, Science and Technology Branch, Environment and Climate Change Canada, Toronto, ON, M3H 5T4, Canada
[3]Key Laboratory of Marine Environment and Ecology (MoE) and Frontiers Sci Ctr Deep Ocean Multispheres & Earth, Ocean University of China, Qingdao, China
10 [4]Qingdao Eco-Environment Monitoring Center of Shandong Province, Qingdao, China
[5]Laboratory for Marine Ecology and Environmental Sciences, Qingdao National Laboratory for Marine Science and Technology, Qingdao, China

Correspondence to: Leiming Zhang (leiming.zhang@ec.gc.ca), Xiaohong Yao (xhyao@ouc.edu.cn)

Abstract. In this study, three methods including the random forest (RF) algorithm, boosted regression trees (BRTs) and the
15 improved complete ensemble empirical mode decomposition with adaptive noise (ICEEMDAN) were adopted for investigating emission-driven interannual variations in concentrations of air pollutants including $PM_{2.5}$, PM_{10}, O_3, NO_2, CO, SO_2 and (NO_2+O_3) monitored in six cities in south China from May 2014 to April 2021. The first two methods were used to calculate the deweathered hourly concentrations, and the third one was used to calculate decomposed hourly residuals. To constrain the uncertainties in the calculated deweathered or decomposed hourly values, a self-developed method was applied
20 to calculate the range of the deweathered percentage changes (DePCs) of air pollutant concentrations on an annual scale (each year covers May to the next April). These four methods were combined together to generate emission-driven trends and percentage changes (PCs) during the seven-year period. Consistent trends between the RF-deweathered and BRTs-deweathered concentrations and the ICEEMDAN-decomposed residuals of an air pollutant in a city were obtained in approximately 70% of a total of 42 cases (for seven pollutants in six cities), but consistent PCs calculated from the three
25 methods, defined as standard deviation being smaller than 10% of the corresponding mean absolute value, were obtained in only approximately 30% of all the cases. The remaining cases with inconsistent trends and/or PCs indicated large uncertainties produced by one or more of the three methods. The calculated PCs from the deweathered concentrations and decomposed residuals were thus combined with the corresponding range of DePCs calculated from the self-developed method to gain the robust range of DePCs where applicable. Based on the robust range of DePCs, we identified significant
30 decreasing trends in $PM_{2.5}$ concentration from 2014 to 2020 in Guangzhou and Shenzhen, which were mainly caused by the reduced air pollutant emissions and to a much less extent by weather perturbations. A decreasing or probably decreasing emission-driven trend was identified in Haikou and Sanya with inconsistent PCs, and a stable or no trend was identified in Zhanjiang with positive PCs. For O_3, a significant increasing trend from 2014 to 2020 was identified in Zhanjiang, Shenzhen,

Guangzhou and Haikou. An increasing trend in (NO_2+O_3) was also identified in Zhanjiang and Guangzhou, and an increasing or probably increasing trend in Haikou, suggesting the contributions from enhanced formation of O_3. The calculated PCs from using different methods implied that the emission changes of O_3 precursors and associated atmospheric chemistry likely played a dominant role than did the perturbations from varying weather conditions. Results from this study also demonstrated the necessity of combining multiple decoupling methods in generating emission-driven trends in atmospheric pollutants.

1 Introduction

With rapid economic growth in the past several decades across China, air pollution has become increasingly severe in most parts of the country (Chan and Yao, 2008; He et al., 2002). A turning point emerged in the most recent decade, benefited from stringent emission control measures implemented in China since 2013, such as "Atmospheric Pollution Prevention and Control Action Plan" (APPCAP) (Chen et al., 2020; Vu et al., 2019; Zhang et al., 2020). Trends in long-term monitored pollutants are important indicators of the effectiveness of the emission control policies (Hogrefe et al., 2000; Rao et al., 1997). This is particularly true in China, where air pollutant emissions have not been updated in the annual reports of ecology and environment issued by local governments at the city level since 2014. The Multi-resolution Emission Inventory for China (MEIC) was developed in 2012 by Tsinghua University to estimate anthropological air pollutant emissions, but it was updated every 2-3 years and only up to 2017.

To evaluate existing national emission control strategies in China (such as APPCAP), several studies have analyzed air pollutants concentrations measured at the national monitoring stations (Hu et al., 2021; Xu and Zhang, 2020; Zhao et al., 2021). However, trends and interannual variations in air concentrations of the monitored pollutants were affected by not only emission changes but also varying meteorological conditions and/or weather systems (Dang et al., 2021; Lin et al., 2021; Vu et al., 2019; Zhang et al., 2019a; Zhang et al., 2019b; Zhao et al., 2020; Henneman et al., 2015; Foley et al., 2015; Astitha et al., 2017; Hogrefe et al., 2002). For example, Zhao et al. (2020) reported that the observed large declines in $PM_{2.5}$, SO_2 and CO concentrations on the national scale during the COVID-19 outbreak were primarily caused by poor dispersion meteorological conditions. Vu et al. (2019) argued that the $PM_{2.5}$ target of 60 $\mu g \cdot m^{-3}$ would have not been achieved in Beijing in the winter of 2017 if without the favourable weather conditions for rapid dispersion and precipitation scavenging of air pollutants. Similarly, Lin et al. (2021) suggested that meteorological factors significantly reduced O_3 concentrations from 2013 to 2020 in eastern and central China, as indicated by the reversed O_3 trends after removing the major meteorological effects. It is thus essential to decouple the total trends in pollutants concentrations into portions caused by varying meteorological factors and weather conditions and by emission changes so that the mitigation effects can be evaluated accurately.

In literature, the multiple linear regression (MLR) method is considered as the simplest approach to decouple the effects of meteorological factors from changed emissions on the trends in air pollutants concentrations (Borlaza et al., 2022; Chen et

al., 2020; Li et al., 2019a; Otero et al., 2018; Zhai et al., 2019). However, the MLR analysis sometimes suffers from the auto-correlation inherently existing between different meteorological parameters (Yao et al., 2009). To overcome this weakness, "meteorological normalization" tools have been developed based on statistical modelling (Chen et al., 2020; Gong et al., 2021; Grange and Carslaw, 2019; Li et al., 2020; Xiao et al., 2021; Xue et al., 2020; Zhai et al., 2019). For example, the machine learning techniques, such as the random forest (RF) algorithm and boosted regression trees (BRTs), performed better than the traditional methods like MLR (Carslaw and Taylor, 2009; Grange et al., 2018) or other air quality numerical models like Weather Research and Forecasting-Community Multi-scale Air Quality model (Vu et al., 2019; Foley et al., 2015; Astitha et al., 2017) in analyzing air quality trends and meteorological impacts. These methods have been used widely in relevant studies across China, e.g., in Beijing (Vu et al., 2019), Beijing-Tianjin-Hebei region (Qu et al., 2020) and North China Plain (He et al., 2021b). In the methods mentioned above, meteorological data are a necessity. In contrast, another exiting method called the empirical mode decomposition (EMD) and its updated version the improved complete ensemble empirical mode decomposition with adaptive noise (ICEEMDAN) directly decompose time series of air pollutants concentrations and deduct the perturbation from meteorological factors on the residuals (trend) to some extent (Colominas et al., 2014; Fu et al., 2020). It should be pointed out that, due to the non-linearity of chemical reactions related to air pollutants, none of the existing methods is perfect in decoupling the effects of dominant factors in the total trends of pollutants concentrations. To evaluate the uncertainties in trend analysis, combining results from several different methods are recommended (Hogrefe et al., 2002; Qiu et al., 2022; Xiao et al., 2021; Xue et al., 2020).

The updated global air quality guidelines from World Health Origination (WHO) declared in 2021 brought new challenges to policy makers for establishing more stringent emission control policies, even in the relatively clean regions like south China. For example, air quality in Hainan province needs to be further improved to meet the new WHO standards, and the demonstration of Hainan Free Trade Port and declaration of the province as a National Ecological Civilization Demonstration Zone in China make this task more challenging. Even more challenges exist for the cities in Guangdong province because of their higher air pollutant concentrations than in Hainan (Gong et al., 2021; He et al., 2017; Li et al., 2019b; Zhang et al., 2019b). To accommodate these challenges, the effect of APPCAP needs to be first assessed regionally in south China. For this purpose, we analyzed seven-year (from May 2014 to April 2021) concentration data of six criteria air pollutants ($PM_{2.5}$, PM_{10}, O_3, NO_2, CO and SO_2) as well as the sum of NO_2 and O_3 in six cities in south China, of which two (Haikou and Sanya) are in Hainan province and four (Guangzhou, Shenzhen, Zhuhai and Zhanjiang) are in Guangdong province. Three different analysis methods were used to identify emission-driven interannual variations and perturbations from varying weather conditions. In addition, a self-developed method was further introduced to constrain analysis uncertainties.

2 Materials and methods

2.1 Monitoring stations and monitored air pollutant concentrations and meteorological data

Six cities in south China, including Haikou and Sanya in Hainan Province and Guangzhou, Shenzhen, Zhuhai and Zhanjiang in Guangdong province, were selected in the present study (Fig. 1). There are two monitoring stations in Sanya, four in Zhuhai, five in Haikou, six in Zhanjiang and 11 stations in both Guangzhou and Shenzhen (Fig. 1 and Table S1). The hourly average air quality data for six criteria pollutants ($PM_{2.5}$, PM_{10}, O_3, NO_2, CO and SO_2) were downloaded from the China National Environmental Monitoring Centre (CNEMC, http://www.cnemc.cn/sssj/) for every monitoring station. The city-specific hourly air quality data represent the average of all the stations in the same city. Data before May 2014 were incomplete, and thus, only the data after May 2014 were used for the analysis. One whole year data covered from May to the next April, e.g., the first-year annual average (referred to as 2014 annual average in the discussion below) covered from May 2014 to April 2015, and the last year average (referred to as annual average in 2020 below) covered from May 2020 to April 2021. For a pollutant in a city, 52204–58695 hourly data were available in seven years (Table S2). Note that all concentrations were converted to the values under the standard conditions (273.15K, 1 atm) for consistency. The sum of NO_2 and O_3 was also analyzed together with the six pollutants mentioned above, and their sum was calculated by considering their different molecular weights, i.e., $[NO_2+O_3] = [NO_2]*48/46 + [O_3]$. Note that concentrations of volatile organic carbons (VOCs) were not reported by CNEMC and this group of pollutants is not considered in the present study. Thus, a total of 42 cases (seven pollutants in six cities) were analysed for deweathered trends.

Hourly meteorological data including wind speed (ws), wind direction (wd), air temperature (at), relative humidity (rh) and dew point (dp) were obtained from the meteorological observational station at a nearby airport (Fig. 1 and Table S1), which are accessible from the NOAA Integrated Surface Database (ISD) by using the "worldmet" R package (Carslaw, 2021). To improve the performance of machine learning models (Hou et al., 2022; Shi et al., 2021), other meteorological parameters, including boundary layer height (blh), total cloud cover (tcc), surface net solar radiation (ssr), surface pressure (sp), and total precipitation (tp), which were extracted from the European Centre for Medium Weather Forecasting's Reanalysis-5 (ERA5) hourly data (https://cds.climate.copernicus.eu/), and air mass clusters based on the Hybrid Single-Particle Lagrangian Integrated Trajectory (HYSPLIT) 72-hour back trajectories at hourly resolution (https://www.ready.noaa.gov/HYSPLIT_traj.php) were also used including for modelling. The meteorological data of each city, ERA5 hourly data and the calculated back trajectories were combined with city-specific hourly air quality data as input for the machine learning analysis.

2.2 Data analysis methods

Two machine learning methods, including the RF algorithm and the BRTs, were separately used to calculate the deweathered hourly concentrations. The third method, the ICEEMDAN, was used to decompose hourly residuals of air pollutants. The Mann-Kendall (M-K) method was then applied to the deweathered and decomposed values to extract the trends and calculate the percentage changes (PCs). A self-developed method was further applied to calculate the range of the deweathered percentage changes (DePCs) of air pollutant concentrations in annual scale. The three PCs and DePCs were

130 combined for constraining the uncertainties and generating a robust range of DePCs. Fig. 2 shows the framework of this study with the four methods to be applied.

The RF algorithm was performed based on the "rmweather" R package (Grange et al., 2018) and the "ranger" R package (Wright and Ziegler, 2017), and the BRTs was performed based on the "deweather" R package (Carslaw et al., 2012; Carslaw and Taylor, 2009). The application of these packages has been well documented in literature, e.g., analyzing long-

135 term trends in concentrations of air pollutants (Grange and Carslaw, 2019; Ma et al., 2021; Mallet, 2020), assessing impact of clean air actions (Vu et al., 2019; Zhang et al., 2020), and evaluating the response of air quality during the COVID-19 lockdown (Dai et al., 2021; Shi and Brasseur, 2020; Wang et al., 2020; Munir et al., 2021; Lovric et al., 2021). The independent input variables to the two machine learning methods include temporal variables (hour, day, weekday, week and month), meteorological parameters (ws, wd, at, rh, dp, blh, tcc, ssr, sp and tp) and monitored pollutant concentrations. The

140 top three most influential meteorological variables in each modeling scenario are listed in Table S3. The inputs were randomly divided into two groups: the training dataset that account for 80% of the data and a testing dataset that contained the remaining 20%. The performance was evaluated by statistical metrics included the correlation coefficient (R^2), root mean square error (RMSE), mean bias (MB), mean fractional bias (MFB) and mean fractional error (MFE). The formulas used to calculate RMSE, MB, MFB and MFE are as follows:

145

$$\text{RMSE} = \sqrt{\frac{\sum_{i=1}^{N}(P_i - O_i)^2}{N}} \qquad \text{(Equation-1)}$$

$$\text{MB} = \frac{1}{N}\sum_{i=1}^{N}(P_i - O_i) \qquad \text{(Equation-2)}$$

$$\text{MFB} = \frac{2}{N}\sum_{i=1}^{N}\left(\frac{P_i - O_i}{P_i + O_i}\right) \times 100\% \qquad \text{(Equation-3)}$$

$$\text{MFE} = \frac{2}{N}\sum_{i=1}^{N}\left(\frac{|P_i - O_i|}{P_i + O_i}\right) \times 100\% \qquad \text{(Equation-4)}$$

in which P_i and O_i represent the ith predicted and observed values, N represents the number of data used to test. Note that

150 United States Environmental Protection Agency (USEPA) proposed the criteria and goal values for MFE and MFB to evaluate the air quality modelling performance, which are MFE≤75% and MFB≤±60% for criteria and MFE≤50% and MFB≤±30% for goal (USEPA, 2007). No such criteria value has been set for the other parameters defined in the above equations.

The indices of PM$_{2.5}$ in Guangzhou are shown as an example in Fig. 3, and the summary of all air pollutants in the six cities

155 can be found in Table S4. In Fig. 3, the minimum RMSE values obtained for the PM$_{2.5}$ test in Guangzhou and used for the final calculation are 12.1 (RF algorithm) and 12.3 (BRTs), respectively. R^2 values are 0.93 (RF algorithm) and 0.91 (BRTs), respectively, implying that the predicted values of PM$_{2.5}$ by the two methods well reproduce the observations. The MB values are -0.22 (RF algorithm) and 0.01 (BRTs), respectively, implying that the BRTs better reproduced the observations than RF algorithm in this case. Note that MB of zero would indicate an ideal prediction. The calculated MB being deviated

160 from zero implies the deweathered hourly concentrations being suffered from the errors to some extent, and the errors would automatically transfer into the deweathered trends and PCs. MFB and MFE values were less than 30% and 50%, respectively,

for both RF algorithm and BRTs (Fig. 3), satisfying the goal values set by USEPA. This suggests well performance in reproducing observations using the two methods, as listed in Table S4. Note that the two machine learning methods always underpredicted $PM_{2.5}$ concentrations in cases with high $PM_{2.5}$ levels, although such cases occurred infrequently. Such an underprediction has also been reported in air quality model predicted $PM_{2.5}$ concentrations, which could be due to missing mechanisms enhancing formation of $PM_{2.5}$ under poor dispersion conditions (Chang et al., 2020; Liu et al., 2021a; Zheng et al., 2015; Shen et al., 2022). In these circumstances, the training for two machine learning methods may not be sufficient to yield good prediction.

In the two machine learning methods, the meteorologically normalized air pollutant concentrations at a particular time were calculated by averaging 1000 model predictions with meteorological variables randomly resampled from the study period (2014−2020), following the approach proposed by (Hou et al., 2022).

$$y_{dew} = \frac{1}{1000}\sum_{i=1}^{1000} x_{i,pred} \qquad \text{(Equation-5)}$$

where $x_{i,pred}$ is the model-predicted concentration for a given meteorological condition at time i, and y_{dew} is the corresponding deweathered hourly concentration at a particular time under averaged meteorological condition. In this study, the deweathered hourly concentrations by the BRTs contained more spikes than those by the RF method. Some of the spikes may be caused by episodic emissions such as agriculture biomass burning, wild forest fires, holiday fireworks, construction activities (Video S1) and accidents and associated enhanced secondary pollution (Chen et al., 2017; Dai et al., 2021; Enayati et al., 2021; Chen et al., 2021; Shen et al., 2022), etc. Meteorological data from the nearest airport in every city were used as input for the two machine learning methods, as has been the choice in most existing studies (Vu et al., 2019; Mallet, 2020; Wang et al., 2020; Dai et al., 2021; Ma et al., 2021). The data should reflect synoptic weather conditions and be suitable for modelling hourly pollutant concentrations averaged from multiple sites in a city.

The ICEEMDAN method (Colominas et al., 2014), which is an improved version of the EMD method, overcomes the "end-effect" originally existing in EMD, providing modes with less noise and avoiding the spurious modes. The original data can be decomposed and expressed as:

$$x = \sum_{i=1}^{k} d_i + r \qquad \text{(Equation 6)}$$

where x is the original data, d_i is the ith intrinsic mode function (IMF), k is the total number of IMFs, and r is the final residual. This method has been applied in various fields, such as financial prediction (Zhou and Chen, 2021) and air quality assessment (Luo et al., 2020). The implementation of the ICEEMDAN method is based on a Python package named PyEMD (Laszuk, 2017). The number of modes needs to be pre-set in this method, which was chosen based on sensitivity test results with the following two criteria: 1) only one oscillation cycle should be kept in the real residual; and 2) combining the real residual and the final mode would end up two or more oscillation cycles. For example, the decomposed residual plus the last mode was finally used as the real ICEEMDAN-decomposed residual for $PM_{2.5}$ in Guangzhou, Shenzhen, Zhanjiang and Zhuhai (Fig. S1a-d, f) while the decomposed residual was used directly as the real ICEEMDAN-decomposed residual for $PM_{2.5}$ in Haikou (Fig. S1e). Note that the ICEEMDAN method requires a complete time series of data. Approximately 5%

data were missing for each air pollutant in each city (Table S2), but the missing data did not occur at the identical hour in two consecutive days, except PM_{10} concentration in Zhanjiang. For the special cases of PM_{10} in Zhanjiang, the missing data were replaced by the average values of the observed data between the nearest day before and after at the identical hour. This approach of replacing missing data may introduce a small uncertainty on the decomposed residuals.

In this study, we also developed a novel method to study emission-driven interannual variations in air pollutant concentrations by calculating the range of DePC on an annual scale based on an earlier approach proposed by Yao and Zhang (2020) (referred to the self-developed method in the present study). Details of this method are presented in the Supplement, with an example of calculating the range of DePC of $PM_{2.5}$ concentration between two years (May 2020 – April 2021 relative to May 2014 – April 2015) in Guangzhou (Table S5 and Fig. S2). There are five steps in this method, including 1) reconstructing the time series of data in any two years to the same size; 2) conducting correlation analysis using the reconstructed data in any two years and removing outliers after the inflection point (Fig. S2); 3) repeating step 2) to remove more outliers; 4) calculating the range of DePC; and 5) evaluating residual perturbations by varying weather conditions. The main advantages of this method include 1) avoiding the calculation of the deweathered hourly concentrations or decomposed hourly residuals of air pollutants in which their uncertainties are unpredictable; 2) confirming the accuracy of DePC when the range of DePC is sufficiently narrow; and 3) identifying the large perturbation from varying weather conditions on DePC when the range of DePC is broad.

The M-K analysis is employed to resolve the trends in the time series of the annual average concentration of each pollutant. Qualitative trend results revolved by the M-K method include 1) an increasing/decreasing trend with a P value of <0.05; 2) a probably increasing/decreasing trend with a P value of 0.05–0.1; 3) a stable trend with a P value of >0.1 as well as with a ratio of <1.0 between the standard deviation and the mean of the dataset; and 4) a no-trend for P>0.1 with all the other conditions (Aziz et al., 2003; Kampata et al., 2008; Yao and Zhang, 2020).

3 Results and discussion

3.1 Trends and PCs of $PM_{2.5}$ and PM_{10}

The seven-year (2014–2020) average mass concentrations of $PM_{2.5}$ were the highest in Guangzhou at 34 $\mu g \cdot m^{-3}$, followed by 27 $\mu g \cdot m^{-3}$ in Shenzhen, 26 $\mu g \cdot m^{-3}$ in Zhanjiang and Zhuhai, 20 $\mu g \cdot m^{-3}$ in Haikou and 15 $\mu g \cdot m^{-3}$ in Sanya (Table 1). The annual average $PM_{2.5}$ concentrations in most cities and in nearly all the years (Table S6) exceeded the annual average Class-I level (15 $\mu g \cdot m^{-3}$) of Ambient Air Quality Standards (AAQS) in China, and exceeded the latest WHO air quality guideline values by several times.

The largest decrease in the annual average $PM_{2.5}$ mass concentration from the first year (2014) to the last year (2020) occurred in Guangzhou, i.e., by 17 $\mu g \cdot m^{-3}$ (or 39%) (Table 1 and Fig. 4). A significant decreasing trend was also identified during the seven-year period by the M-K method (p<0.05). A similar case was also found in Shenzhen with a decrease of 9 $\mu g \cdot m^{-3}$ (or 28%) from 2014 to 2020 and a significant decreasing trend (p<0.05) during the same period. However, a probably

decreasing trend (0.05≤p<0.1) or a stable trend (p≥0.1) was revealed by the M-K method in the other four cities. Note that a 20%–40% decrease in $PM_{2.5}$ annual average concentrations was frequently observed across China since 2013, e.g., a nationwide decrease by an overall 22% from 2015 to 2018 (Zhao et al., 2021), an approximate 40% decrease in Beijing and 20% decrease in Pearl River Delta from 2015 to 2019 (Hu et al., 2021; Xu and Zhang, 2020).

To explore the emission-driven trends in $PM_{2.5}$ concentration in the six cities, the RF-deweathered and BRTs-deweathered $PM_{2.5}$ concentrations and the ICEEMDAN-decomposed residuals of $PM_{2.5}$ concentrations are examined in Fig. 4a-l. In Guangzhou and Shenzhen, a consistent decreasing trend (p<0.05) was identified by the M-K method in the deweathered $PM_{2.5}$ concentrations and the decomposed residuals of $PM_{2.5}$ concentrations (Table 1 and Fig. 4a and b). The PCs from 2014 to 2020 were also reasonably consistent between the different datasets mentioned above (Table 2), i.e., with the standard deviation of the three PCs being within 10% of the corresponding mean absolute value. Specifically, the PCs from 2014 to 2020 in Shenzhen calculated from the RF-deweathered and BRTs-deweathered $PM_{2.5}$ concentrations and the ICEEMDAN-decomposed residuals were -35%, -34% and -30%, respectively, which were not much different from that using the original $PM_{2.5}$ concentration (28% as discussed above). A combination of these four PCs values in Shenzhen allowed to infer that: 1) the reduced air pollutant emissions in Shenzhen and upwind regions likely decreased the $PM_{2.5}$ concentrations by 33% ± 3% (mean ± standard deviation) from 2014 to 2020, and 2) the perturbation from varying weather conditions cancelled out 5% ± 3% out of the of 33% ± 3% decrease. In Guangzhou, the PCs of $PM_{2.5}$ concentrations from 2014 to 2020 estimated by the three methods were -33% (RF-deweathered), -35% (BRTs-deweathered) and -35% (ICEEMDAN-decomposed), while the PCs calculated from the original annual average $PM_{2.5}$ concentrations was -39%, as mentioned above. Thus, the reduced emissions of air pollutants in Guangzhou and upwind regions likely decreased the concentrations of $PM_{2.5}$ by 34% ± 1% during the seven-year period, while the perturbation from varying weather conditions caused an additional decrease of 5% ± 1%. Gong et al. (2021) also reported an additional 5% decrease driven by varying meteorological conditions, on top of the 47% decrease driven by reduced emissions, in the national annual averages of $PM_{2.5}$ mass concentration from 2013 to 2019 in China.

A decreasing trend (p<0.05) was also identified in Zhuhai, Haikou and Sanya when using the RF-deweathered and BRTs-deweathered concentrations and the ICEEMDAN-decomposed residuals (Table 1 and Fig. 4d-e, j-l), which are in contrast with probably decreasing trends generated from using the original $PM_{2.5}$ concentration data. The perturbations from varying weather conditions on $PM_{2.5}$ mass concentrations likely complicated the effects of reduced air pollutant emissions in the three cities and upwind regions during 2014–2020. It is noted that the PCs estimated from the three different methods (RF-deweathered, BRTs-deweathered and ICEEMDAN-decomposed) varied little for Sanya (-23%, -21% and -24%) and Haikou (-19%, -20% and -20%) from 2014 to 2020, but quite large for Zhuhai (-38%, -37% and -26%), the latter case was likely due to the large uncertainties associated with one or more methods (Table 2). We revealed the most influential meteorological factors on the RF-predicted and BRTs-predicted concentrations, which was surface pressure in 7 out of 12 cases, followed by relative humidity in 3 out of 12 cases, dew point in one case, and air temperature in one case (Table S3). However, the

260   influence of surface pressure on pollutants concentrations was poorly understood, and so is the case of its role on interpreting uncertainties in modelling results.

A no-trend or stable trend was identified for Zhanjiang (Table 1, Fig. 4c and i), regardless of which method was used. The PCs from 2014 to 2020 were all positive, i.e., 14% (RF-deweathered), 3% (BRTs-deweathered), 5% (ICEEMDAN-decomposed), and 8% (original data), indicating emission-driven increases in $PM_{2.5}$ concentration in this city during this

265   period.

Similar analysis to the one discussed above was also conducted on PM_{10} concentrations (Tables 1 and 2 and Fig. S3a-l), results from which can be summarized below.

1) The highest seven-year (2014–2020) average PM_{10} concentrations of 57 $\mu g \cdot m^{-3}$ occurred in Guangzhou, followed by 45 $\mu g \cdot m^{-3}$ in Shenzhen, 43 $\mu g \cdot m^{-3}$ in Zhuhai, 42 $\mu g \cdot m^{-3}$ in Zhanjiang, 37 $\mu g \cdot m^{-3}$ in Haikou and 29 $\mu g \cdot m^{-3}$ in Sanya. The

270   annual average PM_{10} concentrations exceeded the annual average Class-I level (40 $\mu g \cdot m^{-3}$) of AAQS in China in most cities and most years, and exceeded the latest WHO air quality guideline values by 2–4 times.

2) The M-K analyses showed either a no or stable trend during 2014–2020 if using the original annual average PM_{10} concentrations in the six cities (Table 1). Inconsistent trends were then obtained by using the three different methods (RF-deweathered, BRTs-deweathered and ICEEMDAN-decomposed) in five out of the six cities. The only exception is

275   for Guangzhou in which a decreasing trend was identified from all of the three methods, although a no trend was extracted from the original annual average concentrations. For Shenzhen, a decreasing trend was obtained using the RF-deweathered method while a probably decreasing or stable trend was obtained from the BRTs-deweathered and ICEEMDAN-decomposed method. For Sanya, a decreasing trend was obtained using the RF-deweathered and the ICEEMDAN-decomposed method, while a no-trend was obtained using the BRTs-deweathered method. The

280   inconsistency between the trends extracted by the three different methods was mostly because the actual interannual changes, and thus the magnitudes of the trends, were small, which are on the same order of magnitude to the methodology uncertainties. Combining all the trends generated using the three different methods and the original data, we concluded a slightly decreasing or stable trend in emission-driven PM_{10} concentrations for all the cities.

3) The PCs of PM_{10} concentration from 2014 to 2020 in Guangzhou were consistent between using the three different

285   methods e.g., -15% (RF-deweathered), -13% (BRTs-deweathered) and -15% (ICEEMDAN-decomposed), while that from using the original PM_{10} concentration data, -11%. Thus, reduced emissions of air pollutants in Guangzhou and upwind regions likely decreased PM_{10} concentrations by 14% ± 1% during the seven-year period, while the perturbation from varying weather conditions cancelled out 3% ± 1%. The reasonably consistent PCs were also obtained for Shenzhen, Zhanjiang and Sanya, although with inconsistent decreasing trends. However, inconsistent PCs were obtained

290   from the three different methods for the other three cities due to methodology uncertainties and the actual small trends, as explained above.

3.2 Trends and PCs of O_3, NO_2 and (NO_2+O_3)

Among the four gaseous criteria pollutants, O_3 concentrations in the six cities exceeded the most, on percentage basis, the Class-I levels of AAQS in China (Table S6). Trend analyses were conducted for both O_3 and (NO_2+O_3) considering the titration reaction of O_3 with NO to form NO_2 in ambient air (Chan and Yao, 2008; Li et al., 2019a; Seinfeld and Pandis, 1998; Sicard et al., 2020; Wang et al., 2017).

The seven-year (2014–2020) average concentrations of O_3 were highest at 69 $\mu g \cdot m^{-3}$ in Zhanjiang and Zhuhai, followed by 62 $\mu g \cdot m^{-3}$ in Shenzhen, 60 $\mu g \cdot m^{-3}$ in Haikou, 58 $\mu g \cdot m^{-3}$ in Sanya (Table 1), and the lowest at 51 $\mu g \cdot m^{-3}$ in Guangzhou. The titration reaction of O_3 with NO likely decreased O_3 concentrations to some extent in Guangzhou, as implied by the highest annual average NO_2 concentrations in this city among the six cities (Table 1). In contrast, the highest O_3 annual averages occurred in Zhanjiang and Zhuhai. The annual average NO_2 concentrations in the two cities were smaller than that in Guangzhou, but larger than that in Sanya. Thus, both the reduced depletion of O_3 via the titration reaction and the enhanced photochemical formation of O_3 likely contributed to the highest annual average O_3 concentrations in the two cities (He et al., 2021a; Liu et al., 2021b; Shen et al., 2021).

Using the original data of annual average O_3 concentrations (Table 1 and Fig. 5a-f), the M-K analysis results showed an increasing trend in Zhanjiang, Shenzhen, Haikou and Guangzhou ($p<0.05$), and a no- trend in Zhuhai and Sanya. Using the RF-deweathered concentrations, the BRTs-deweathered concentrations and the ICEEMDAN-decomposed residuals (Fig. 5a-l and Fig. S1g-l), M-K analysis results generated the same trend as mentioned above in every city. Thus, the emission-driven increasing trends in O_3 concentration from 2014 to 2020 can be firmly confirmed in four cities (Zhanjiang, Shenzhen, Haikou and Guangzhou).

The PCs of the deweathered concentrations, the decomposed residuals, and the original annual average concentrations from 2014 to 2020 in the four cities with increasing trends of O_3 concentration were further analyzed, and were presented below from the largest to the smallest PCs. In Haikou, the PCs from 2014 to 2020 was 65% based on the original annual average O_3 concentrations (Table 2). The corresponding PCs were 54%, 65% and 64% based on the RF-deweathered concentrations, the BRTs-deweathered concentrations, and the ICEEMDAN-decomposed residuals, respectively. Combining these numbers together, we concluded that the emission changes of O_3 precursors and associated changes in atmospheric chemistry likely increased the O_3 concentration by at least 54% from 2014 to 2020, and the perturbations from varying weather conditions seemingly yielded an additional increase of 0%–11%. Similarly, in Guangzhou, Shenzhen and Zhanjiang, the emission changes of O_3 precursors likely increased the concentrations of O_3 by 26%±1.5%, >10% and >17%, respectively, from 2014 to 2020, and the perturbations from varying weather conditions seemingly yielded an additional increase of 14%±1.5%, 8%–18% and -1%–14%, respectively.

In the case of NO_2, Guangzhou is the only city having annual average NO_2 concentrations exceeding the annual average Class-I level of AAQS in China (40 $\mu g \cdot m^{-3}$) in most of the years; the only exception is in 2020 mostly due to reduced emissions as a result of COVID-19 pandemic (Bauwens et al., 2020; Shi and Brasseur, 2020; Wang et al., 2020; Wang et al., 2021; Zhao et al., 2020). Annual average NO_2 concentrations were below 40 $\mu g \cdot m^{-3}$ in all the other cities during all the years, but were far above the latest WHO air quality guideline value of 10 $\mu g \cdot m^{-3}$. When the seven-year (2014–2020) average NO_2

concentrations in six cities were compared, the value of 46 μg·m^{-3} in Guangzhou ranked at the top, followed by 30 μg·m^{-3} in Shenzhen, 29 μg·m^{-3} in Zhuhai, 15 μg·m^{-3} in Zhanjiang and Haikou, and lowest at 12 μg·m^{-3} in Sanya (Table 1).

A decreasing trend in NO_2 concentration from 2014 to 2020 was obtained in Shenzhen and Zhuhai based on the deweathered concentrations and the decomposed residuals, while a probably decreasing trend was obtained based on the original annual average concentration data (Fig. S5a-l). In Shenzhen, the PCs in NO_2 from 2014 to 2020 were mostly consistent between the different methods (Table 2), e.g., -18% (RF-deweathered), -20% (BRTs-deweathered), -21% (ICEEMDAN-decomposed) and -21% (original data). However, this was not the case in Zhuhai for which the four PCs were -17% (RF-deweathered), -16% (BRTs-deweathered), -8% (ICEEMDAN-decomposed) and -18% (original annual average). A stable trend in NO_2 concentration from 2014 to 2020 was obtained in Guangzhou, regardless of the method used. The impact of the reduced NO_x emissions in Guangzhou and/or upwind areas could not be detected in the observed NO_2 concentrations on annual scale. Inconsistent trends were obtained between using different methods in Zhanjiang, Haikou and Sanya, similar to the cases of several other pollutants discussed above and below.

Combining NO_2 and O_3 together, an increasing trend ($p<0.05$, Table 2) was obtained from 2014 to 2020 in Haikou, while probably increasing, no-trend or stable trends were obtained in the other five cities based on the original annual average concentration data (Fig. S4a-l). A consistent increasing trend in (NO_2+O_3) was obtained in Guangzhou and Zhanjiang based on any of the RF-deweathered concentrations, BRTs-deweathered concentrations, and decomposed residuals of (NO_2+O_3). In Haikou, an increasing trend was obtained based on the RF-deweathered and BRTs-deweathered concentrations while a probably increasing trend was obtained from the decomposed residuals. The increasing trends in (NO_2+O_3) from 2014 to 2020 in the above-mentioned three cities confirmed the enhanced formation of O_3. However, either no or stable trends were obtained in Zhuhai, Shenzhen and Sanya based on the deweathered concentrations or the decomposed residuals of (NO_2+O_3) (Table 1). The contrasting trends between (NO_2+O_3) and O_3 in Shenzhen, i.e., a no-trend in the former and an increasing trend in the latter (Table 1), was likely due to the reduced O_3 depletion via the titration reaction of O_3 by NO.

The PCs in (NO_2+O_3) from 2014 to 2020 in Haikou, Guangzhou and Zhanjiang were presented below from the largest to the smallest PCs. In Haikou, the PCs were estimated to be 39%, 55%, 48% and 62% based on the RF-deweathered concentrations, the BRTs-deweathered concentrations, the ICEEMDAN-decomposed residual and the original annual average concentrations, respectively. Thus, the 39%–55% O_3 increases from 2014 to 2020 were likely attributed to the emission-driven enhanced O_3 formation. In addition, the first three PCs values for (NO_2+O_3) were smaller than those of O_3 by 10%–16%, which represented the reduced O_3 depletion via the titration reaction (Li et al., 2019a; Wang et al., 2017). In Guangzhou, the estimated four PCs in (NO_2+O_3) were 11% (RF-deweathered), 7% (BRTs-deweathered), 15% (ICEEMDAN-decomposed) and 15% (original data). These numbers were smaller than those for O_3 by 11%–25%, implying similar contributions from the reduced O_3 depletion via the titration reaction and the enhanced O_3 formation to the total increased O_3 concentration. In Zhanjiang, the estimated four PCs in (NO_2+O_3) were 18%, 13%, 20% and 14%, which are mostly similar to those for O_3 (18%, 17%, 32% and 18%) (Table 2), implying the dominate contribution of the enhanced O_3 formation to the increased O_3 concentration.

3.3 Trends and PCs of CO and SO₂

The annual average concentrations of CO and SO_2 were all below the Class-I levels of AAQS in China during 2014–2020 in all the cities (Table 1). A consistent decreasing trend in annual average CO concentration was obtained, regardless which method was used, in all the cities except Haikou (Fig. S6a-l). A consistent decreasing trend in annual average SO_2 concentration was also obtained using the four different methods in Shenzhen and Zhuhai. In Guangzhou, a decreasing trend in annual average SO_2 concentration was obtained based on the deweathered concentrations and decomposed residuals, while a probably decreasing trend was obtained based on the original annual average data (Fig. S7a-l). In Sanya, an increasing trend in annual average SO_2 concentration was obtained based on the deweathered concentrations and decomposed residuals, while a probably increasing trend was obtained based on the original annual average data. In Haikou and Zhanjiang, inconsistent trends were obtained between using the deweathered concentrations and decomposed residuals.

The reasonably consistent PCs in annual average CO concentration from 2014 to 2020 between using different methods were only obtained in Shenzhen and Zhanjiang, i.e., -40% and -32% (RF-deweathered), -36% and -34% (BRTs-deweathered), -39% and -32% (ICEEMDAN-decomposed), and -36% and -34% (original data), respectively. The PCs in SO_2 from 2014 to 2020 were reasonably consistent between using different methods in Guangzhou and Zhuhai, e.g., the four values in Guangzhou were -46% (RF-deweathered), -46% (BRTs-deweathered), -47% (ICEEMDAN-decomposed) and -44% (original average).

3.4 Constraining analysis uncertainties

Of the 42 cases analyzed in this study, approximately 70% showed consistent trends from 2014 to 2020 between using the RF-deweathered concentrations, the BRTs-deweathered concentrations and the ICEEMDAN-decomposed residuals as input to the M-K analysis. The remaining 30% with inconsistent trends were apparently caused by methodology uncertainties in some or all of the three methods (RF, BRTs and ICEEMDAN). The PCs from 2014 to 2020 using the same three data sets, although mostly comparable, were only absolutely consistent in approximately 30% of the cases. Thus, the PCs calculated from the above three methods were further assessed using the range of DePCs using the self-developed method introduced in Section 2. Even for the consistent cases, additional examination using an independent method is still valuable to exclude potential coincidence.

The PCs of $PM_{2.5}$ from 2014 to 2020 varied from -35% to -33% in Guangzhou and from -35% to -30% in Shenzhen as discussed in Section 3. After applying the self-developed method, the corresponding DePCs were estimated to be in the range of -37% – -33% in Guangzhou and -36% – -31% in Shenzhen. The overlap portion between the range of PCs and the range of DePCs in each city was thereby set up as the robust range of DePCs, i.e., -35% – -33% in Guangzhou, and -35% – -31% in Shenzhen (Table 2). The robust ranges of DePCs were almost the same as those of PCs in both cities, further confirming the emission-driven PCs and the perturbation from varying weather conditions presented in Section 3. These cases were referred to as Category 1-a below.

The PCs of $PM_{2.5}$ from 2014 to 2020 were from -20% to -19% in Haikou and from -24% to -21% in Sanya. The corresponding DePC had no overlap with these PCs ranges in these cities, implying nonexistence of a robust range of DePC. These cases were referred to as Category 1-b below. Note that the self-developed method would not introduce additional observational variables in the calculation process as shown in Text S1 and Fig S2, and the true DePC should be within the range of DePC calculated using the self-developed method. The consistent results obtained from the deweathered concentrations and decomposed residual in Category 1-b were likely ascribed to a coincidence, and may be invalid.

The PCs of $PM_{2.5}$ from 2014 to 2020 were in a relatively large range in Zhuhai and Zhanjiang, implying certain extent of inconsistence between the three methods (RF, BRTs, and ICEEMDAN). The PCs in Zhuhai varied from -38% to -26%, and the corresponding DePC had no overlap with this range, implying non-existence of a robust range of DePC. This case was referred to as Category 2-a below. Similar to Category 1-b, the deweathered and decomposed methods cannot reasonably estimate the perturbation from varying weather conditions in Category 2-a. The PCs in Zhanjiang ranged from 3% to 14%, and the corresponding DePC completely overlapped this range, again confirming the emission-driven PCs and the perturbation from varying weather conditions presented in Section 3. This case was referred to as Category 2-b below.

The PCs of PM_{10} from 2014 to 2020 were inconsistent between using the RF-deweathered concentrations, the BRTs-deweathered concentrations and the ICEEMDAN-decomposed residuals of PM_{10} in Zhuhai. Nevertheless, a robust range of DePCs was obtained in Zhuhai (-20% – -14%). Comparing the robust range of DePCs with the range of PCs calculated using the original annual average data (-21%), the perturbation from varying weather conditions yielded an additional decrease in PM_{10} concentration by 1%–7% in Zhuhai. This case was refereed as Category 2-c below, featuring a narrower robust range of DePCs than that of PCs calculated from the deweathered concentrations and decomposed residuals. PM_{10} in Sanya, Shenzhen, Zhanjiang and Guangzhou followed into Category 1-a, confirming the emission-driven PCs and the perturbation from varying weather conditions. PM_{10} in Haikou followed into Category 2-a with no robust range of DePC.

O_3 in Haikou, Shenzhen and Zhuhai followed into Category 2-c, and that in Guangzhou, Zhanjiang and Sanya followed into Category 1-a, 2-a and 2-b, respectively. Results of (NO_2+O_3), NO_2, CO and SO_2 also followed into some of the five categories (Table 2), and the above interpretation for $PM_{2.5}$, PM_{10} and O_3 in each category on the emission-driven PCs and the perturbation from varying weather conditions are also applicable to the (NO_2+O_3), NO_2, CO and SO_2.

4 Conclusions

In this study, we first applied separately the RF algorithm, the BRTs algorithm, and the ICEEMDAN to obtain time series of the deweathered concentrations or decomposed residuals of criteria air pollutants and (NO_2+O_3) from May 2014 to April 2021 in the six cities in south China. We found that the RF-deweathered and BRTs-deweathered concentrations and the ICEEMDAN-decomposed residuals yielded consistent trends in approximately 70% of the cases. We then calculated the PCs between the first and the last year using the above-mentioned deweathered concentrations and residuals. Only in approximately 30% of the cases the PCs were reasonably consistent between the three methods, indicating large

methodology uncertainties in one or more methods. The self-developed method was further used to calculate the range of
425   DePCs, and a robust range of DePCs was identified in approximately 70% of the cases.

Based on those consistent trends obtained from the different methods and the robust range of DePCs, we finally generated the following findings.

1)   Significant decreasing trends in $PM_{2.5}$ concentration during 2014–2020 were identified in Guangzhou and Shenzhen, which were mainly caused by the reduced air pollutant emissions and to a much less extent by weather perturbations. A
430   stable or no trend in $PM_{2.5}$ was identified in Zhanjiang, implying no detectable effects of the reduced air pollutant emissions on the monitored $PM_{2.5}$. A decreasing or probably decreasing emission-driven trends were obtained in the remaining cities. The emission-driven effects likely took the lead in the overall changes, although uncertainties associated with one or more methods still existed on basis of inconsistent PCs.

2)   Increasing trends in O_3 concentration during 2014–2020 were identified in Zhanjiang, Shenzhen, Guangzhou and
435   Haikou. The emission changes of O_3 precursors played a dominant role than did the perturbations from varying weather conditions. However, increasing trends in (NO_2+O_3) were only identified in Zhanjiang, Guangzhou and Haikou with increasing and probably increasing trends obtained from different methods, which also confirmed the different contribution ratios of the reduced O_3 depletion via the titration reaction and the enhanced formation of O_3.

This study demonstrates the necessity of combining multiple decoupling and/or trend analysis methods in order to constrain
440   the uncertainties in trend analysis results inherent in any individual method. Interpretation of trend analysis results presented in this study could be strengthened if detailed discussions on atmospheric processes and chemistry mechanisms were provided, which unfortunately could not be accommodated here due to the lack of reliable long-term data of concerned chemical species, such as the major chemical components in $PM_{2.5}$ and PM_{10}, VOCs and up-to-date emission inventory of all the involved pollutants. A lack of knowledge of the detailed city-level mitigation measures on air pollutants also limited our
445   capacity for providing a comprehensive assessment of the existing clean air policies.

Acknowledgement

This work was supported by Hainan Provincial Natural Science Foundation of China (grant no.422MS098), Natural Science Foundation of China (grant no. 41776086) and Hainan Provincial Postgraduate Innovative Research Project (grant no. Yhys2021-5).
450

Code and data availability. The code of DePC calculation can be accessed via https://pypi.org/project/DePC/, the data used in this paper are downloadable from http://www.cnemc.cn/sssj/.

Author contribution. XY and LZ designed the research. YL and QF carried out the measurement and analyzed the data. All
455 authors provided comments and contributed to the text.

Competing interests. The authors declare that they have no conflict of interest.

References

460 Astitha, M., Luo, H., Rao, S. T., Hogrefe, C., Mathur, R., and Kumar, N.: Dynamic evaluation of two decades of WRF-CMAQ ozone
     simulations over the contiguous United States, Atmos Environ, 164, 102-116. https://doi.org/10.1016/j.atmosenv.2017.05.020, 2017.
     Aziz, J. J., Ling, M., Rifai, H. S., Newell, C. J., and Gonzales, J. R.: MAROS: a decision support system for optimizing monitoring plans,
     Ground Water, 41, 355-367. https://doi.org/10.1111/j.1745-6584.2003.tb02605.x, 2003.
     Bauwens, M., Compernolle, S., Stavrakou, T., Muller, J. F., van Gent, J., Eskes, H., Levelt, P. F., van der, A. R., Veefkind, J. P., Vlietinck,
465   J., Yu, H., and Zehner, C.: Impact of coronavirus outbreak on NO_2 pollution assessed using TROPOMI and OMI observations,
     Geophys Res Lett, 47, e2020GL087978. https://doi.org/10.1029/2020GL087978, 2020.
     Borlaza, L. J., Weber, S., Marsal, A., Uzu, G., Jacob, V., Besombes, J.-L., Chatain, M., Conil, S., and Jaffrezo, J.-L.: Nine-year trends of
     PM_{10} sources and oxidative potential in a rural background site in France, Atmos Chem Phys, 22, 8701-8723.
     https://doi.org/10.5194/acp-22-8701-2022, 2022.
470 Carslaw, D. C.: Worldmet: Import Surface Meteorological Data from NOAA Integrated Surface Database (ISD), R package version 0.9.5,
     https://cran.r-project.org/package=worldmet. 2021.
     Carslaw, D. C. and Taylor, P. J.: Analysis of air pollution data at a mixed source location using boosted regression trees, Atmos Environ,
     43, 3563-3570. https://doi.org/10.1016/j.atmosenv.2009.04.001, 2009.
     Carslaw, D. C., Williams, M. L., and Barratt, B.: A short-term intervention study — Impact of airport closure due to the eruption of
475   Eyjafjallajökull on near-field air quality, Atmos Environ, 54, 328-336. https://doi.org/10.1016/j.atmosenv.2012.02.020, 2012.
     Chan, C. K. and Yao, X. H.: Air pollution in mega cities in China, Atmos Environ, 42, 1-42.
     https://doi.org/10.1016/j.atmosenv.2007.09.003, 2008.
     Chang, Y., Huang, R. J., Ge, X., Huang, X., Hu, J., Duan, Y., Zou, Z., Liu, X., and Lehmann, M. F.: Puzzling Haze Events in China
     During the Coronavirus (COVID-19) Shutdown, Geophys Res Lett, 47, e2020GL088533. https://doi.org/10.1029/2020GL088533,
480   2020.
     Chen, J., Li, C., Ristovski, Z., Milic, A., Gu, Y., Islam, M. S., Wang, S., Hao, J., Zhang, H., He, C., Guo, H., Fu, H., Miljevic, B.,
     Morawska, L., Thai, P., Lam, Y. F., Pereira, G., Ding, A., Huang, X., and Dumka, U. C.: A review of biomass burning: Emissions
     and impacts on air quality, health and climate in China, Sci Total Environ, 579, 1000-1034.
     https://doi.org/10.1016/j.scitotenv.2016.11.025, 2017.
485 Chen, L., Zhu, J., Liao, H., Yang, Y., and Yue, X.: Meteorological influences on $PM_{2.5}$ and O_3 trends and associated health burden since
     China's clean air actions, Sci Total Environ, 744, 140837. https://doi.org/10.1016/j.scitotenv.2020.140837, 2020.
     Chen, X. K., Jiang, Z., Shen, Y. N., Li, R., Fu, Y. F., Liu, J., Han, H., Liao, H., Cheng, X. G., Jones, D. B. A., Worden, H., and González
     Abad, G.: Chinese regulations are working - why is surface ozone over industrialized areas still high? Applying lessons from
     Northeast US air quality evolution, Geophys Res Lett, 48, e2021GL092816. https://doi.org/10.1029/2021gl092816, 2021.
490 Colominas, M. A., Schlotthauer, G., and Torres, M. E.: Improved complete ensemble EMD: A suitable tool for biomedical signal
     processing, Biomed Signal Proces, 14, 19-29. https://doi.org/10.1016/j.bspc.2014.06.009, 2014.
     Dai, Q. L., Hou, L. L., Liu, B. W., Zhang, Y. F., Song, C. B., Shi, Z. B., Hopke, P. K., and Feng, Y. C.: Spring Festival and COVID-19
     lockdown:disentangling PM sources in major Chinese cities, Geophys Res Lett, 48, e2021GL093403.
     https://doi.org/10.1029/2021gl093403, 2021.
495 Dang, R. J., Liao, H., and Fu, Y.: Quantifying the anthropogenic and meteorological influences on summertime surface ozone in China
     over 2012-2017, Sci Total Environ, 754, 142394. https://doi.org/10.1016/j.scitotenv.2020.142394, 2021.
     Enayati, A. F., Pakbin, P., Hasheminassab, S., Epstein, S. A., Li, X., Polidori, A., and Low, J.: Long-term trends of $PM_{2.5}$ and its carbon
     content in the South Coast Air Basin: A focus on the impact of wildfires, Atmos Environ, 255.
     https://doi.org/10.1016/j.atmosenv.2021.118431, 2021.

500 Foley, K. M., Hogrefe, C., Pouliot, G., Possiel, N., Roselle, S. J., Simon, H., and Timin, B.: Dynamic evaluation of CMAQ part I: Separating the effects of changing emissions and changing meteorology on ozone levels between 2002 and 2005 in the eastern US, Atmos Environ, 103, 247-255. https://doi.org/10.1016/j.atmosenv.2014.12.038, 2015.

Fu, H. Y., Zhang, Y. T., Liao, C., Mao, L., Wang, Z. Y., and Hong, N. N.: Investigating $PM_{2.5}$ responses to other air pollutants and meteorological factors across multiple temporal scales, Sci Rep-Uk, 10, 15639. https://doi.org/10.1038/s41598-020-72722-z, 2020.

505 Gong, S. L., Liu, H. L., Zhang, B. H., He, J. J., Zhang, H. D., Wang, Y. Q., Wang, S. X., Zhang, L., and Wang, J.: Assessment of meteorology vs. control measures in the China fine particular matter trend from 2013 to 2019 by an environmental meteorology index, Atmos Chem Phys, 21, 2999-3013. https://doi.org/10.5194/acp-21-2999-2021, 2021.

Grange, S. K. and Carslaw, D. C.: Using meteorological normalisation to detect interventions in air quality time series, Sci Total Environ, 653, 578-588. https://doi.org/10.1016/j.scitotenv.2018.10.344, 2019.

510 Grange, S. K., Carslaw, D. C., Lewis, A. C., Boleti, E., and Hueglin, C.: Random forest meteorological normalisation models for Swiss PM_{10} trend analysis, Atmos Chem Phys, 18, 6223-6239. https://doi.org/10.5194/acp-18-6223-2018, 2018.

He, G., Deng, T., Wu, D., Wu, C., Huang, X. F., Li, Z. N., Yin, C. Q., Zou, Y., Song, L., Ouyang, S. S., Tao, L. P., and Zhang, X.: Characteristics of boundary layer ozone and its effect on surface ozone concentration in Shenzhen, China: A case study, Sci Total Environ, 791, 148044. https://doi.org/10.1016/j.scitotenv.2021.148044, 2021a.

515 He, J. J., Gong, S. L., Yu, Y., Yu, L. J., Wu, L., Mao, H. J., Song, C. B., Zhao, S. P., Liu, H. L., Li, X. Y., and Li, R. P.: Air pollution characteristics and their relation to meteorological conditions during 2014-2015 in major Chinese cities, Environ Pollut, 223, 484-496. https://doi.org/10.1016/j.envpol.2017.01.050, 2017.

He, K. B., Huo, H., and Zhang, Q.: Urban Air Pollution in China: Current Status, Characteristics, and Progress, Annu Rev Energy Environ, 27, 397-431. https://doi.org/10.1146/annurev.energy.27.122001.083421, 2002.

520 He, Y. X., Pan, Y. P., Gu, M. N., Sun, Q., Zhang, Q. Q., Zhang, R. J., and Wang, Y. S.: Changes of ammonia concentrations in wintertime on the North China Plain from 2018 to 2020, Atmos Res, 253, 105490. https://doi.org/10.1016/j.atmosres.2021.105490, 2021b.

Henneman, L. R. F., Holmes, H. A., Mulholland, J. A., and Russell, A. G.: Meteorological detrending of primary and secondary pollutant concentrations: Method application and evaluation using long-term (2000–2012) data in Atlanta, Atmos Environ, 119, 201-210. https://doi.org/10.1016/j.atmosenv.2015.08.007, 2015.

525 Hogrefe, C., Rao, S. T., Zurbenko, I. G., and Porter, P. S.: Interpreting the Information in Ozone Observations and Model Predictions Relevant to Regulatory Policies in the Eastern United States, B Am Meteorol Soc, 81, 2083-2106. https://doi.org/10.1175/1520-0477(2000)081<2083:itiioo>2.3.co;2, 2000.

Hogrefe, C., Vempaty, S., Rao, S. T., and Porter, P. S.: A comparison of four techniques for separating different time scales in atmospheric variables, Atmos Environ, 37, 313-325. https://doi.org/10.1016/S1352-2310(02)00897-X, 2002.

530 Hou, L. L., Dai, Q. L., Song, C. B., Liu, B. W., Guo, F. Z., Dai, T. J., Li, L. X., Liu, B. S., Bi, X. H., Zhang, Y. F., and Feng, Y. C.: Revealing Drivers of Haze Pollution by Explainable Machine Learning, Environ Sci Tech Let, 9, 112-119. https://doi.org/10.1021/acs.estlett.1c00865, 2022.

Hu, M. M., Wang, Y. F., Wang, S., Jiao, M. Y., Huang, G. H., and Xia, B. C.: Spatial-temporal heterogeneity of air pollution and its relationship with meteorological factors in the Pearl River Delta, China, Atmos Environ, 254, 118415.
535 https://doi.org/10.1016/j.atmosenv.2021.118415, 2021.

Kampata, J. M., Parida, B. P., and Moalafhi, D. B.: Trend analysis of rainfall in the headstreams of the Zambezi River Basin in Zambia, Phys Chem Earth, 33, 621-625. https://doi.org/10.1016/j.pce.2008.06.012, 2008.

Laszuk, D.: PyEMD: Python implementation of Empirical Mode Decomposition algorithm, Python package version 1.2.0, https://pypi.org/project/EMD-signal/. 2017.

540 Li, K., Jacob, D. J., Liao, H., Shen, L., Zhang, Q., and Bates, K. H.: Anthropogenic drivers of 2013-2017 trends in summer surface ozone in China, P Natl Acad Sci USA, 116, 422-427. https://doi.org/10.1073/pnas.1812168116, 2019a.

Li, R., Cui, L. L., Hongbo, F., Li, J. L., Zhao, Y. L., and Chen, J. M.: Satellite-based estimation of full-coverage ozone (O_3) concentration and health effect assessment across Hainan Island, J Clean Prod, 244, 118773. https://doi.org/10.1016/j.jclepro.2019.118773, 2020.

Li, R., Wang, Z. Z., Cui, L. L., Fu, H. B., Zhang, L. W., Kong, L. D., Chen, W. D., and Chen, J. M.: Air pollution characteristics in China
545 during 2015-2016: Spatiotemporal variations and key meteorological factors, Sci Total Environ, 648, 902-915. https://doi.org/10.1016/j.scitotenv.2018.08.181, 2019b.

Lin, C. Q., Lau, A. K. H., Fung, J. C. H., Song, Y. S., Li, Y., Tao, M. H., Lu, X. C., Ma, J., and Lao, X. Q.: Removing the effects of meteorological factors on changes in nitrogen dioxide and ozone concentrations in China from 2013 to 2020, Sci Total Environ, 793, 148575. https://doi.org/10.1016/j.scitotenv.2021.148575, 2021.

550 Liu, X., Chang, M., Zhang, J., Wang, J., Gao, H., Gao, Y., and Yao, X.: Rethinking the causes of extreme heavy winter $PM_{2.5}$ pollution events in northern China, Sci Total Environ, 794, 148637. https://doi.org/10.1016/j.scitotenv.2021.148637, 2021a.

Liu, X. F., Guo, H., Zeng, L. W., Lyu, X. P., Wang, Y., Zeren, Y. Z., Yang, J., Zhang, L. Y., Zhao, S. Z., Li, J., and Zhang, G.: Photochemical ozone pollution in five Chinese megacities in summer 2018, Sci Total Environ, 801, 149603. https://doi.org/10.1016/j.scitotenv.2021.149603, 2021b.

555 Lovric, M., Pavlovic, K., Vukovic, M., Grange, S. K., Haberl, M., and Kern, R.: Understanding the true effects of the COVID-19 lockdown on air pollution by means of machine learning, Environ Pollut, 274, 115900. https://doi.org/10.1016/j.envpol.2020.115900, 2021.

Luo, H. Y., Astitha, M., Hogrefe, C., Mathur, R., and Rao, S. T.: Evaluating trends and seasonality in modeled $PM_{2.5}$ concentrations using empirical mode decomposition, Atmos Chem Phys, 20, 13801-13815. https://doi.org/10.5194/acp-20-13801-2020, 2020.

560 Ma, R. M., Ban, J., Wang, Q., Zhang, Y. Y., Yang, Y., He, M. Z., Li, S. S., Shi, W. J., and Li, T. T.: Random forest model based fine scale spatiotemporal O_3 trends in the Beijing-Tianjin-Hebei region in China, 2010 to 2017, Environ Pollut, 276, 116635. https://doi.org/10.1016/j.envpol.2021.116635, 2021.

Mallet, M. D.: Meteorological normalisation of PM_{10} using machine learning reveals distinct increases of nearby source emissions in the Australian mining town of Moranbah, Atmos Pollut Res. https://doi.org/10.1016/j.apr.2020.08.001, 2020.

565 Munir, S., Luo, Z., and Dixon, T.: Comparing different approaches for assessing the impact of COVID-19 lockdown on urban air quality in Reading, UK, Atmos Res. https://doi.org/10.1016/j.atmosres.2021.105730, 2021.

Otero, N., Sillmann, J., Mar, K. A., Rust, H. W., Solberg, S., Andersson, C., Engardt, M., Bergstrom, R., Bessagnet, B., Colette, A., Couvidat, F., Cuvelier, C., Tsyro, S., Fagerli, H., Schaap, M., Manders, A., Mircea, M., Briganti, G., Cappelletti, A., Adani, M., D'Isidoro, M., Pay, M. T., Theobald, M., Vivanco, M. G., Wind, P., Ojha, N., Raffort, V., and Butler, T.: A multi-model comparison

570 of meteorological drivers of surface ozone over Europe, Atmos Chem Phys, 18, 12269-12288. https://doi.org/10.5194/acp-18-12269-2018, 2018.

Qiu, M., Zigler, C., and Selin, N. E.: Statistical and machine learning methods for evaluating trends in air quality under changing meteorological conditions, Atmos Chem Phys, 22, 10551-10566. https://doi.org/10.5194/acp-22-10551-2022, 2022.

Qu, L. L., Liu, S. J., Ma, L. L., Zhang, Z. Z., Du, J. H., Zhou, Y. H., and Meng, F.: Evaluating the meteorological normalized $PM_{2.5}$ trend

575 (2014-2019) in the "2+26" region of China using an ensemble learning technique, Environ Pollut, 266, 115346. https://doi.org/10.1016/j.envpol.2020.115346, 2020.

Rao, S. T., Zurbenko, I. G., Neagu, R., Porter, P. S., Ku, J. Y., and Henry, R. F.: Space and Time Scales in Ambient Ozone Data, B Am Meteorol Soc, 78, 2153-2166. https://doi.org/10.1175/1520-0477(1997)078<2153:satsia>2.0.co;2, 1997.

Seinfeld, J. H. and Pandis, S. N.: Atmospheric Chemistry and Physics: From Air Pollution to Climate Change, Wiley1998.

580 Shen, H. Q., Liu, Y. H., Zhao, M., Li, J., Zhang, Y. N., Yang, J., Jiang, Y., Chen, T. S., Chen, M., Huang, X. B., Li, C. L., Guo, D. L., Sun, X. Y., Xue, L. K., and Wang, W. X.: Significance of carbonyl compounds to photochemical ozone formation in a coastal city (Shantou) in eastern China, Sci Total Environ, 764, 144031. https://doi.org/10.1016/j.scitotenv.2020.144031, 2021.

Shen, Y., Meng, H., Yao, X., Peng, Z., Sun, Y., Zhang, J., Gao, Y., Feng, L., Liu, X., and Gao, H.: Does Ambient Secondary Conversion or the Prolonged Fast Conversion in Combustion Plumes Cause Severe $PM_{2.5}$ Air Pollution in China?, Atmosphere, 13, 673.

585 https://doi.org/10.3390/atmos13050673, 2022.

Shi, X. Q. and Brasseur, G. P.: The Response in Air Quality to the Reduction of Chinese Economic Activities During the COVID-19 Outbreak, Geophys Res Lett, 47, e2020GL088070. https://doi.org/10.1029/2020GL088070, 2020.

Shi, Z. B., Song, C. B., Liu, B. W., Lu, G. D., Xu, J. S., Vu, T. V., Elliott, R. J. R., Li, W. J., Bloss, W. J., and Harrison, R. M.: Abrupt but smaller than expected changes in surface air quality attributable to COVID-19 lockdowns, Sci Adv, 7.

590 https://doi.org/10.1126/sciadv.abd6696, 2021.

Sicard, P., De Marco, A., Agathokleous, E., Feng, Z., Xu, X., Paoletti, E., Rodriguez, J. J. D., and Calatayud, V.: Amplified ozone pollution in cities during the COVID-19 lockdown, Sci Total Environ, 735, 139542. https://doi.org/10.1016/j.scitotenv.2020.139542, 2020.

USEPA., 2007. Guidance on the Use of Models and Other Analyses for Demonstrating Attainment of Air Quality Goals for Ozone, $PM_{2.5}$,

595 and Regional Haze. EPA-454/B-07-002.

Vu, T. V., Shi, Z. B., Cheng, J., Zhang, Q., He, K. B., Wang, S. X., and Harrison, R. M.: Assessing the impact of clean air action on air quality trends in Beijing using a machine learning technique, Atmos Chem Phys, 19, 11303-11314. https://doi.org/10.5194/acp-19-11303-2019, 2019.

Wang, N., Xu, J. W., Pei, C. L., Tang, R., Zhou, D. R., Chen, Y. N., Li, M., Deng, X. J., Deng, T., Huang, X., and Ding, A. J.: Air Quality

600 During COVID-19 Lockdown in the Yangtze River Delta and the Pearl River Delta: Two Different Responsive Mechanisms to Emission Reductions in China, Environ Sci Technol, 55, 5721-5730. https://doi.org/10.1021/acs.est.0c08383, 2021.

Wang, T., Xue, L. K., Brimblecombe, P., Lam, Y. F., Li, L., and Zhang, L.: Ozone pollution in China: A review of concentrations, meteorological influences, chemical precursors, and effects, Sci Total Environ, 575, 1582-1596. https://doi.org/10.1016/j.scitotenv.2016.10.081, 2017.

605 Wang, Y. J., Wen, Y. F., Wang, Y., Zhang, S. J., Zhang, K. M., Zheng, H. T., Xing, J., Wu, Y., and Hao, J. M.: Four-Month Changes in Air Quality during and after the COVID-19 Lockdown in Six Megacities in China, Environ Sci Tech Let, 7, 802-808. https://doi.org/10.1021/acs.estlett.0c00605, 2020.

Wright, M. N. and Ziegler, A.: ranger: A Fast Implementation of Random Forests for High Dimensional Data in C++ and R, J Stat Softw, 77, 1-17. https://doi.org/10.18637/jss.v077.i01, 2017.

610   Xiao, Q. Y., Zheng, Y. X., Geng, G. N., Chen, C. H., Huang, X. M., Che, H. Z., Zhang, X. Y., He, K. B., and Zhang, Q.: Separating emission and meteorological contributions to long-term $PM_{2.5}$ trends over eastern China during 2000–2018, Atmos Chem Phys, 21, 9475-9496. https://doi.org/10.5194/acp-21-9475-2021, 2021.

Xu, X. H. and Zhang, T. C.: Spatial-temporal variability of $PM_{2.5}$ air quality in Beijing, China during 2013-2018, J Environ Manage, 262, 110263. https://doi.org/10.1016/j.jenvman.2020.110263, 2020.

615   Xue, T., Zheng, Y. X., Geng, G. N., Xiao, Q. Y., Meng, X., Wang, M., Li, X., Wu, N. N., Zhang, Q., and Zhu, T.: Estimating Spatiotemporal Variation in Ambient Ozone Exposure during 2013-2017 Using a Data-Fusion Model, Environ Sci Technol, 54, 14877-14888. https://doi.org/10.1021/acs.est.0c03098, 2020.

Yao, X. H. and Zhang, L. M.: Decoding long-term trends in the wet deposition of sulfate, nitrate, and ammonium after reducing the perturbation from climate anomalies, Atmos Chem Phys, 20, 721-733. https://doi.org/10.5194/acp-20-721-2020, 2020.

620   Yao, X. H., Xu, X. H., Sabaliauskas, K., and Fang, M.: Comment on "Atmospheric particulate matter pollution during the 2008 Beijing Olympics", Environ Sci Technol, 43, 7589; author reply 7590-7581. https://doi.org/10.1021/es902276p, 2009.

Zhai, S. X., Jacob, D. J., Wang, X., Shen, L., Li, K., Zhang, Y. Z., Gui, K., Zhao, T. L., and Liao, H.: Fine particulate matter ($PM_{2.5}$) trends in China, 2013–2018: separating contributions from anthropogenic emissions and meteorology, Atmos Chem Phys, 19, 11031-11041. https://doi.org/10.5194/acp-19-11031-2019, 2019.

625   Zhang, G., Gao, Y., Cai, W. J., Leung, L. R., Wang, S. X., Zhao, B., Wang, M. H., Shan, H. Y., Yao, X. H., and Gao, H. W.: Seesaw haze pollution in North China modulated by the sub-seasonal variability of atmospheric circulation, Atmos Chem Phys, 19, 565-576. https://doi.org/10.5194/acp-19-565-2019, 2019a.

Zhang, X. Y., Xu, X. D., Ding, Y. H., Liu, Y. J., Zhang, H. D., Wang, Y. Q., and Zhong, J. T.: The impact of meteorological changes from 2013 to 2017 on $PM_{2.5}$ mass reduction in key regions in China, Sci China Earth Sci, 62, 1885-1902. https://doi.org/10.1007/s11430-
630   019-9343-3, 2019b.

Zhang, Y. M., Vu, T. V., Sun, J. Y., He, J. J., Shen, X. J., Lin, W. L., Zhang, X. Y., Zhong, J. T., Gao, W. K., Wang, Y. Q., Fu, T. M., Ma, Y. P., Li, W. J., and Shi, Z. B.: Significant Changes in Chemistry of Fine Particles in Wintertime Beijing from 2007 to 2017: Impact of Clean Air Actions, Environ Sci Technol, 54, 1344-1352. https://doi.org/10.1021/acs.est.9b04678, 2020.

Zhao, H., Chen, K. Y., Liu, Z., Zhang, Y. X., Shao, T., and Zhang, H. L.: Coordinated control of $PM_{2.5}$ and O_3 is urgently needed in China
635   after implementation of the "Air pollution prevention and control action plan", Chemosphere, 270, 129441. https://doi.org/10.1016/j.chemosphere.2020.129441, 2021.

Zhao, Y. B., Zhang, K., Xu, X. T., Shen, H. Z., Zhu, X., Zhang, Y. X., Hu, Y. T., and Shen, G. F.: Substantial Changes in Nitrogen Dioxide and Ozone after Excluding Meteorological Impacts during the COVID-19 Outbreak in Mainland China, Environ Sci Tech Let, 7, 402-408. https://doi.org/10.1021/acs.estlett.0c00304, 2020.

640   Zheng, B., Zhang, Q., Zhang, Y., He, K. B., Wang, K., Zheng, G. J., Duan, F. K., Ma, Y. L., and Kimoto, T.: Heterogeneous chemistry: a mechanism missing in current models to explain secondary inorganic aerosol formation during the January 2013 haze episode in North China, Atmos Chem Phys, 15, 2031-2049. https://doi.org/10.5194/acp-15-2031-2015, 2015.

Zhou, J. G. and Chen, D. F.: Carbon Price Forecasting Based on Improved CEEMDAN and Extreme Learning Machine Optimized by Sparrow Search Algorithm, Sustainability-Basel, 13, 4896. https://doi.org/10.3390/su13094896, 2021.
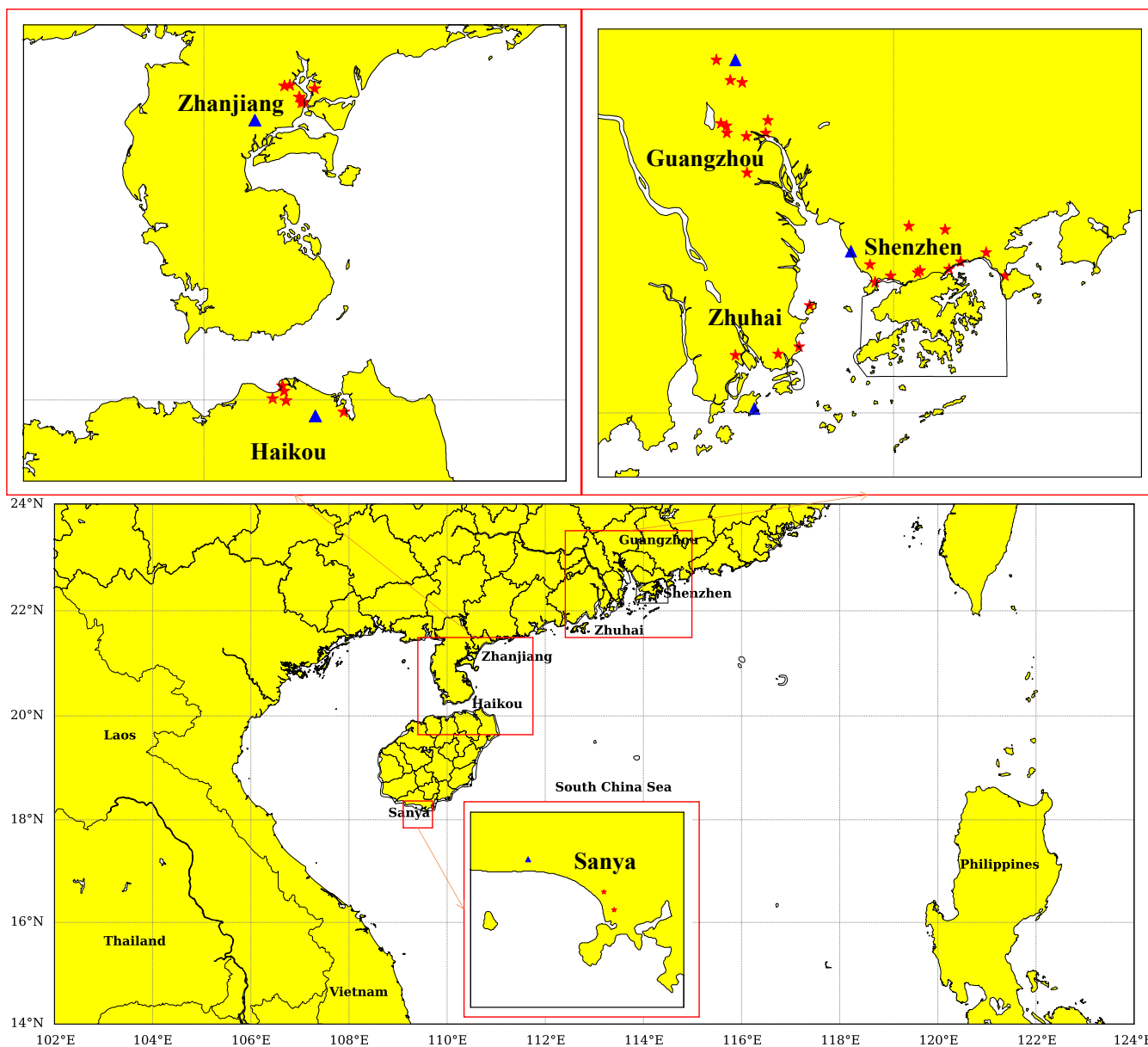
Figure 1: Maps of the study areas and locations of air quality monitoring stations (red star) and one meteorological station (blue triangle) in each city.
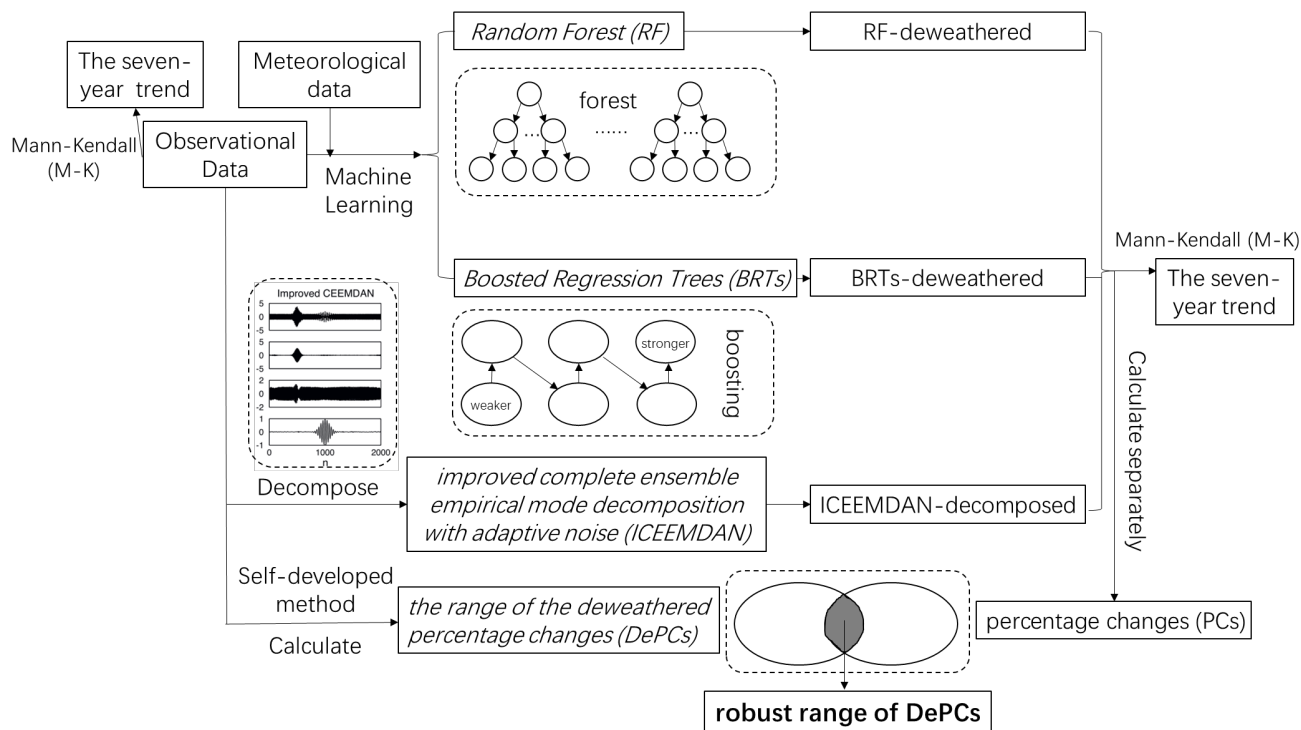
Figure 2: The framework of this study on the four methods to be applied.

650
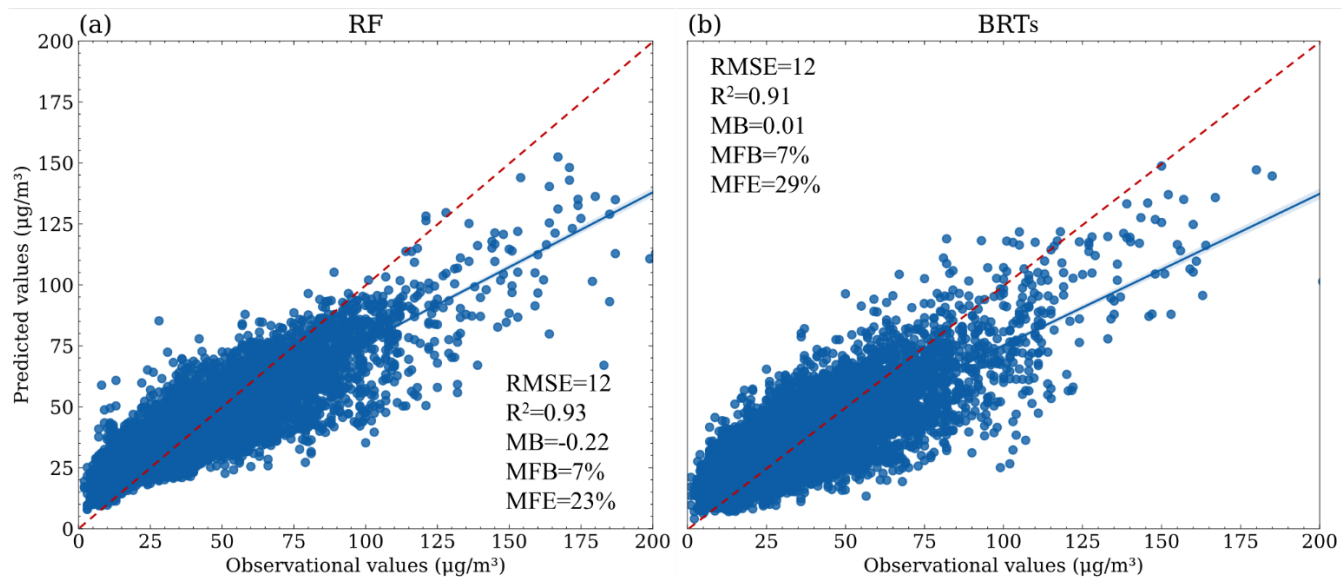
Figure 3: The performance of PM₂.₅ predictions of the two machine learning methods in Guangzhou. (a) RF-deweathered, (b) BRTs-deweathered.

655
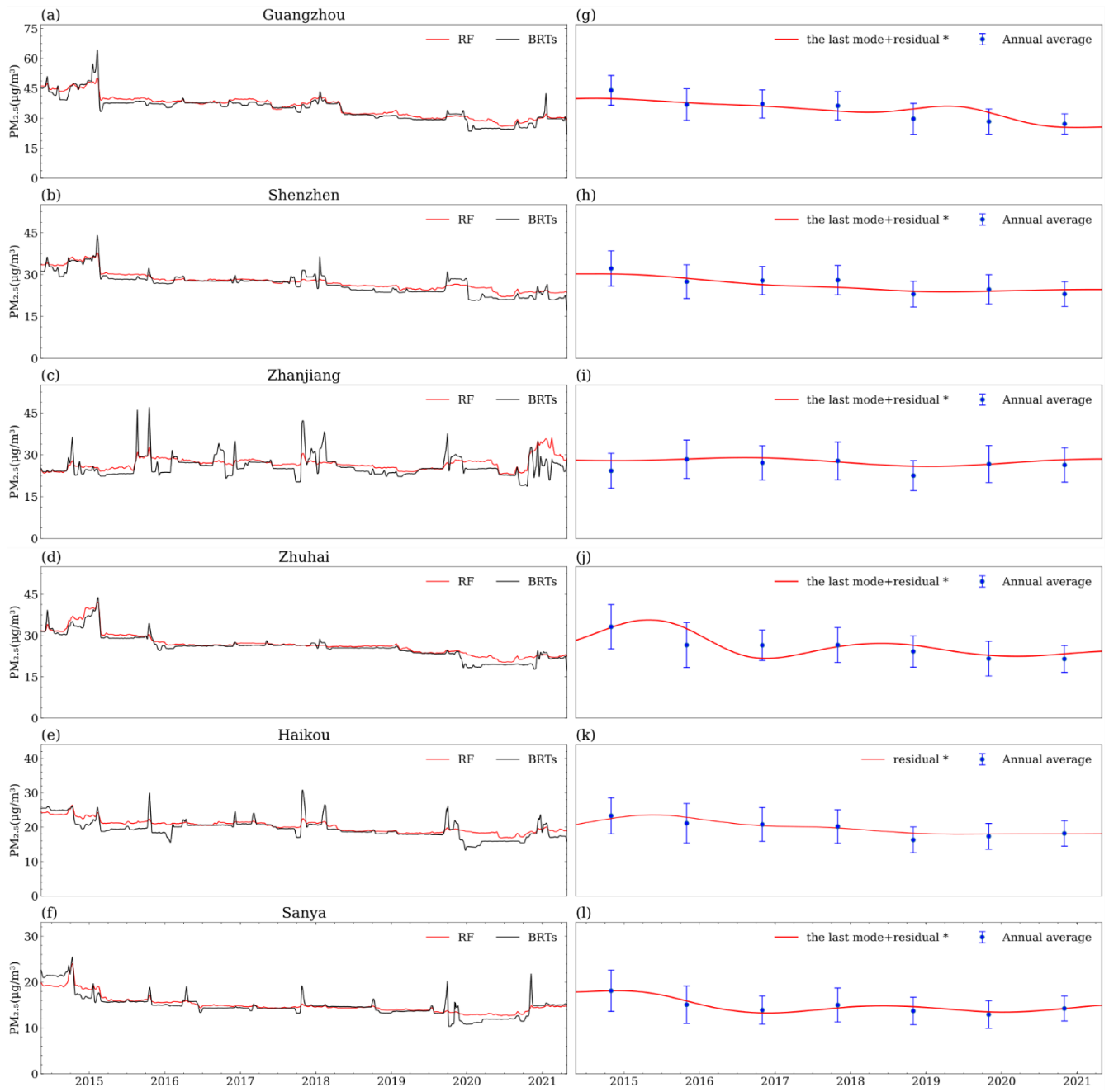
Figure 4: The RF-deweathered and BRTs-deweathered concentrations, ICEEMDAN-decomposed residuals (or mode + residuals) of PM$_{2.5}$ and annual averages from May 2014 to April 2021. a-f: deweathered concentrations in the six cities (the order of the cities is same as that listed in Table 1); g-l: decomposed residual or (the last mode + residual) and annual averages plus one-third standard deviation in the six cities (* represents the time series of values to be used to calculate the trend and PC).

660
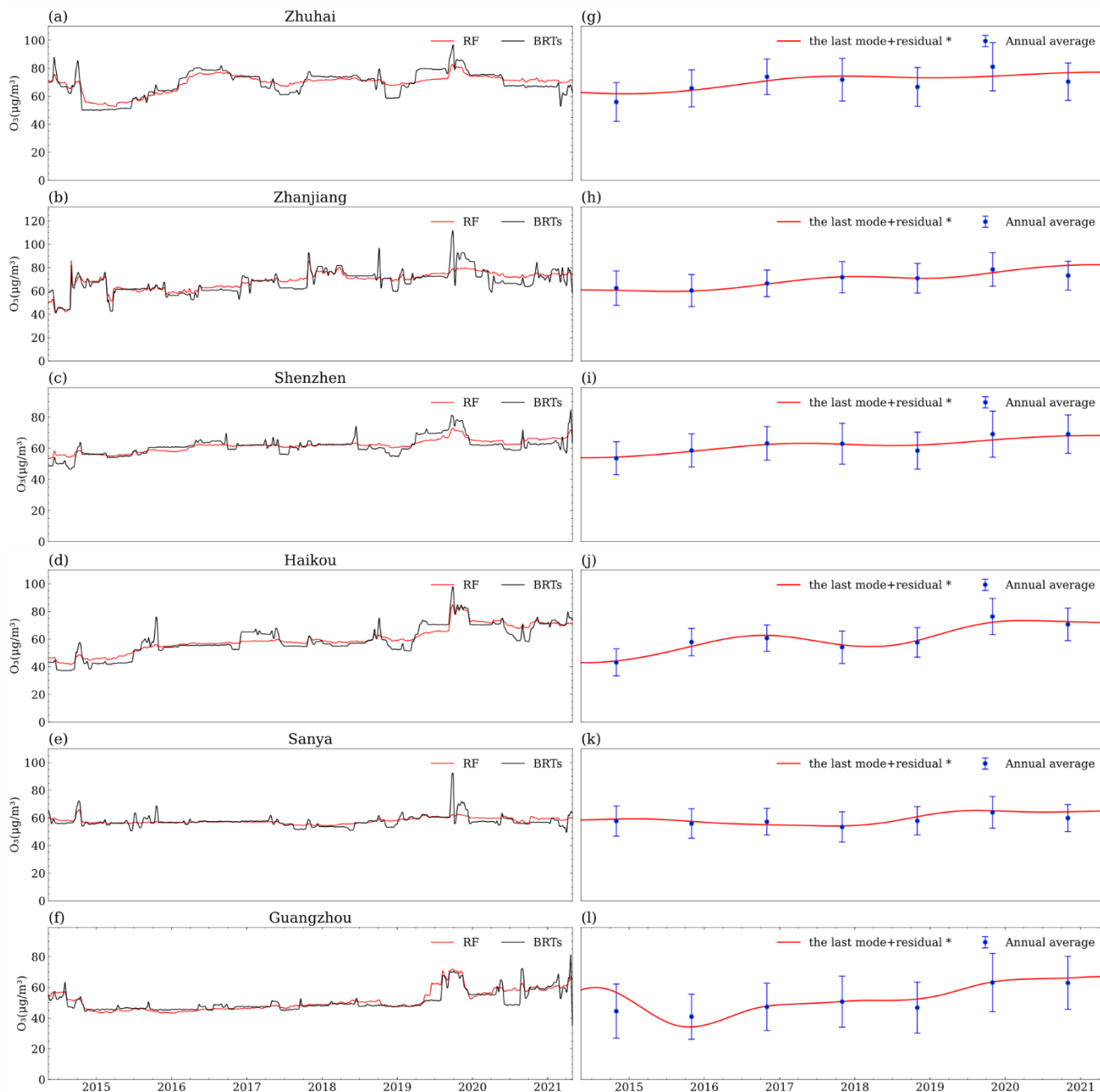
Figure 5: Same as Figure 4, except the pollutant to be O₃.

Table 1: The original annual average concentrations of six criteria air pollutants and (NO₂+O₃) and their trends in original annual averages, RF-deweathered and BRTs-deweathered concentrations and ICEEMDAN-decomposed residuals in six cities detected by the M-K method.

Pollutant	city	seven-year average	2014	2015	2016	2017	2018	2019	2020	original trend	RF	BRTs	ICEE-MDAN
PM$_{2.5}$ (µg·m⁻³)	Guangzhou	34	44	37	37	36	30	28	27	↓*	↓*	↓*	↓*
	Shenzhen	27	32	27	28	28	23	25	23	↓*	↓*	↓*	↓*
	Zhanjiang	26	24	28	27	28	23	27	26	—	N	—	N
	Zhuhai	26	33	27	26	27	24	22	21	↓	↓*	↓*	↓*
	Haikou	20	23	21	21	20	16	17	18	↓	↓*	↓*	↓*
	Sanya	15	18	15	14	15	14	13	14	↓	↓*	↓*	↓*
PM$_{10}$ (µg·m⁻³)	Guangzhou	57	63	59	60	57	49	55	56	N	↓*	↓*	↓*
	Shenzhen	45	56	44	44	46	39	44	45	—	↓*	↓	—
	Zhuhai	43	53	48	43	43	36	37	42	N	↓*	↓*	—
	Zhanjiang	42	50	44	43	43	35	40	42	N	↓	↓*	—
	Haikou	37	42	39	39	37	32	34	35	N	↓*	↓*	—
	Sanya	29	34	28	28	29	29	29	27	—	↓*	N	↓*
O$_3$ (µg·m⁻³)	Zhuhai	69	56	66	74	72	67	81	70	N	N	N	N
	Zhanjiang	69	62	60	66	72	71	78	73	↑*	↑*	↑*	↑*
	Shenzhen	62	54	59	63	63	58	69	69	↑*	↑*	↑*	↑*
	Haikou	60	43	58	61	54	58	76	71	↑*	↑*	↑*	↑*
	Sanya	58	58	56	57	53	58	64	60	N	N	N	N
	Guangzhou	51	45	41	47	51	47	63	63	↑*	↑*	↑*	↑*
NO$_2$+O$_3$ (µg·m⁻³)	Zhuhai	100	91	100	106	103	98	103	100	N	N	N	—
	Guangzhou	99	92	88	101	103	95	110	106	—	↑*	↑*	↑*
	Shenzhen	93	89	93	96	93	86	97	97	N	N	N	N
	Zhanjiang	85	79	77	81	88	86	94	90	↑	↑*	↑*	↑*
	Haikou	76	58	75	75	68	71	91	94	↑*	↑*	↑*	↑
	Sanya	70	72	68	68	66	68	74	72	N	N	N	N
NO$_2$ (µg·m⁻³)	Guangzhou	46	46	45	52	50	46	45	40	—	—	—	—
	Shenzhen	30	34	33	32	29	27	27	27	↓	↓*	↓*	↓*
	Zhuhai	29	34	33	31	29	30	21	28	↓	↓*	↓*	↓*
	Zhanjiang	15	16	16	14	15	14	15	16	—	—	—	N
	Haikou	15	15	16	14	13	13	14	18	N	N	—	↑*
	Sanya	12	14	12	11	12	10	10	12	—	—	—	↓*
CO (mg·m⁻³)	Guangzhou	0.90	0.99	0.95	0.93	0.85	0.86	0.84	0.85	↓*	↓*	↓*	↓*
	Zhanjiang	0.77	1.01	0.87	0.79	0.72	0.68	0.66	0.67	↓*	↓*	↓*	↓*
	Shenzhen	0.76	1.04	0.82	0.80	0.68	0.64	0.65	0.67	↓*	↓*	↓*	↓*
	Zhuhai	0.66	0.81	0.68	0.71	0.61	0.63	0.58	0.60	↓*	↓*	↓*	↓*
	Haikou	0.63	0.73	0.66	0.62	0.61	0.60	0.65	0.58	↓	↓	—	↓*
	Sanya	0.52	0.56	0.61	0.52	0.51	0.49	0.49	0.44	↓*	↓*	↓*	↓*
SO$_2$ (µg·m⁻³)	Guangzhou	11	15	11	12	12	7	8	9	↓	↓*	↓*	↓*
	Zhanjiang	8	10	7	9	8	6	9	9	—	—	—	↓*
	Shenzhen	7	9	8	8	8	6	6	7	↓*	↓*	↓*	↓*
	Zhuhai	7	8	10	9	8	5	4	6	↓*	↓*	↓*	↓*
	Haikou	6	6	6	6	6	5	5	5	↓	↓*	—	—
	Sanya	4	3	4	3	3	4	4	4	↑	↑*	↑*	↑*

↑* (↓*): Increasing (Decreasing) trend, i.e., $p < 0.05$;
↑ (↓): Probably increasing (decreasing) trend, i.e., $0.05 \leq p < 0.1$;
—: Stable trend;
N: No trend.

Table 2: The PCs of six criteria pollutants and (NO₂+O₃) calculated from original averages, RF-deweathered and BRTs-deweathered concentrations and ICEEMDAN-decomposed residuals and the robust ranges of DePC in six cities (units in %, * represents no robust DePC).

Pollutant	city	original	RF	BRTs	ICEE-MDAN	DePC range	final range
PM$_{2.5}$	Guangzhou	-39	-33	-35	-35	[-37, -33]	[-35, -33]
	Zhuhai	-36	-38	-37	-26	[-41, -39]	*
	Shenzhen	-28	-35	-34	-30	[-36, -31]	[-35, -31]
	Haikou	-22	-19	-20	-20	[-27, -26]	*
	Sanya	-22	-23	-21	-24	[-39, -30]	*
	Zhanjiang	8	14	3	5	[5,13]	[5, 13]
PM$_{10}$	Zhuhai	-21	-27	-24	-9	[-20, -14]	[-20, -14]
	Sanya	-21	-26	-27	-28	[-27, -23]	[-27, -26]
	Shenzhen	-20	-23	-22	-21	[-28, -15]	[-23, -21]
	Haikou	-17	-19	-16	-13	[-21, -20]	*
	Zhanjiang	-16	-23	-20	-22	[-22, -21]	[-22, -21]
	Guangzhou	-11	-15	-13	-15	[-18, -11]	[-15, -13]
O$_3$	Haikou	65	54	65	64	[43,59]	[54, 59]
	Guangzhou	40	28	25	26	[19,34]	[25, 28]
	Shenzhen	28	19	20	10	[20, 26]	[20, 20]
	Zhuhai	25	16	10	17	[14, 15]	[14, 15]
	Zhanjiang	18	18	17	32	[-16, 5]	*
	Sanya	3	0	1	7	[0, 4]	[0, 4]
NO$_2$+O$_3$	Haikou	62	39	55	48	[49, 65]	[49, 55]
	Guangzhou	15	11	7	15	[5,10]	[7, 10]
	Zhanjiang	14	18	13	20	[-15, 5]	*
	Zhuhai	10	6	3	-1	[1,23]	[1, 6]
	Shenzhen	9	3	3	3	[3,16]	[3, 3]
	Sanya	0	-1	-1	0	[-3, -1]	[-1, -1]
NO$_2$	Shenzhen	-21	-18	-20	-21	[-22, -22]	*
	Zhuhai	-18	-17	-16	-8	[-26,0]	[-17, -8]
	Sanya	-14	-10	-14	-9	[-19, -4]	[-14, -9]
	Guangzhou	-13	-4	-11	-13	[-13, -12]	[-13, -13]
	Zhanjiang	0	0	-2	9	[0,6]	[0, 6]
	Haikou	20	21	16	7	[14,36]	[14, 21]
CO	Shenzhen	-36	-40	-36	-39	[-39, -38]	[-39, -38]
	Zhanjiang	-34	-32	-34	-32	[-62, -26]	[-34, -32]
	Zhuhai	-26	-28	-26	-32	[-32, -24]	[-32, -26]
	Sanya	-22	-21	-18	-14	[-20, -14]	[-20, -14]
	Haikou	-20	-34	-17	-12	[-15, -7]	[-15, -12]
	Guangzhou	-14	-14	-14	-19	[-29, -17]	[-19, -17]
SO$_2$	Guangzhou	-44	-46	-46	-47	[-75, -50]	*
	Zhuhai	-34	-40	-37	-40	[-59, -47]	*
	Shenzhen	-22	-24	-23	-32	[-70, -18]	[-32, -23]
	Haikou	-19	-18	-16	-20	[-25, -20]	[-20, -20]
	Zhanjiang	-16	-20	-14	-25	[-22, -5]	[-22, -14]
	Sanya	75	68	76	98	[83, 94]	[83, 94]